Comprehensive numerical modeling of raceways in blast furnaces

Chemical Engineering Science 289 (2024) 119857

Contents lists available at ScienceDirect

Chemical Engineering Science

journal homepage: www.elsevier.com/locate/ces

Comprehensive numerical modeling of raceways in blast furnaces

Chih-Chia Huang [a], Stefan Born [b], Margot Klaassen [b], Jeroen A. van Oijen [a,c], Niels G. Deen [a,c], Yali Tang [a,c,*]

[a] Power & Flow group, Department of Mechanical Engineering, Eindhoven University of Technology, PO Box 513, 5600 MB, Eindhoven, the Netherlands
[b] Research and Development, Engineering Department, Tata Steel, Ijmuiden, the Netherlands
[c] Eindhoven Institute of Renewable Energy Systems (EIRES), Eindhoven University of Technology, PO Box 513, 5600 MB, Eindhoven, the Netherlands

ARTICLE INFO

Keywords:
Blast furnaces
Raceway
CFD-DEM
FGM
Pulverized coal
Coke
Bird's nest
Combustion
Transient simulations

ABSTRACT

A numerical investigation of dynamic raceway formation in an industrial-scale blast furnace is performed using Computational Fluid Dynamics (CFD) coupled with a Discrete Element Method (DEM). The industrial-scale simulations are made feasible by incorporating the Flamelet Generated Manifold (FGM) method and a coarse-graining method to reduce the computational cost while ensuring effective modeling of gas phase combustion and a large number of solid particles, respectively. The model considers the interactions between pulverized coal (PC) and coke, as well as their interaction with gas. The simulations reveal a different size and shape of the physical and chemical raceway, indicating that not all crucial reactions occur within the physical raceway. According to the model, the physical raceway formation is primarily determined by the blast air momentum, and the PC combustion has a negligible effect on its dimensions. The chemical raceway formation heavily depends on the oxidation rate of coke. The utilization of PC is quantified in terms of burnout. Smaller PC particles are found to undergo a higher degree of burnout due to faster convective heating and oxidation rates. Modifying the angle of the PC injection lance in current configuration is found to be inconsequential to PC burnout. The presented results highlight the significance of enhancing PC-blast mixing to improve PC utilization and provide new insights into optimizing blast furnace operations.

1. Introduction

Blast furnaces (BFs) have been the primary process for producing iron globally, with over 70% of the steel consumed worldwide being produced through this process (IEA, 2022; Geerdes et al., 2020). The production of pig iron from BFs involves the reduction of iron ore using CO (and H_2), which is generated from the use of coke and pulverized coal (PC). The heavy reliance on solid fossil fuels in BFs contributes to over 5% of the global CO_2 emissions from the energy sector (IEA, 2020). Although the steel industry is transitioning towards a more sustainable and renewable energy-based economy, the use of coke and coal in BF remains prevalent until a full transition is achieved. It is important for this transition to be as clean as possible, in order to limit the rise of global temperature within 1.5 °C to pre-industrial levels, as per the 2021 Glasgow agreement (UNFCCC, 2021). Therefore, reducing greenhouse gas emissions from BFs has become a priority for the ironmaking industry.

In the lower part of the BFs, hot blast with PC is injected into a coke bed, creating a void region known as the raceway. The formation of the raceway is essential to BFs operation, as coke and PC are co-combusted to provide heat and the reducing gas CO (and H_2) required for the reduction and melting process above. A high coal combustion efficiency in the raceway is desirable in order to reduce feed costs and prevent unburnt coal from accumulating in the coke bed, forming an impermeable zone that could impede flow of gas or hot metal. More importantly, a high coal combustion efficiency can reduce the dependence on coking coals, thereby reducing the carbon footprint of BFs. Therefore, a thorough understanding of the thermochemical behavior and dynamics of the raceway evolution is essential for coal economics as well as sustainability. However, getting insights into raceway phenomena has been challenging due to the harsh conditions, i.e., high temperature

* Corresponding author at: Power & Flow group, Department of Mechanical Engineering, Eindhoven University of Technology, PO Box 513, 5600 MB, Eindhoven, the Netherlands.
E-mail address: y.tang2@tue.nl (Y. Tang).
URL: https://www.tue.nl/en/research/researchers/yali-tang (Y. Tang).

https://doi.org/10.1016/j.ces.2024.119857
Received 26 October 2023; Received in revised form 12 January 2024; Accepted 4 February 2024
Available online 9 February 2024

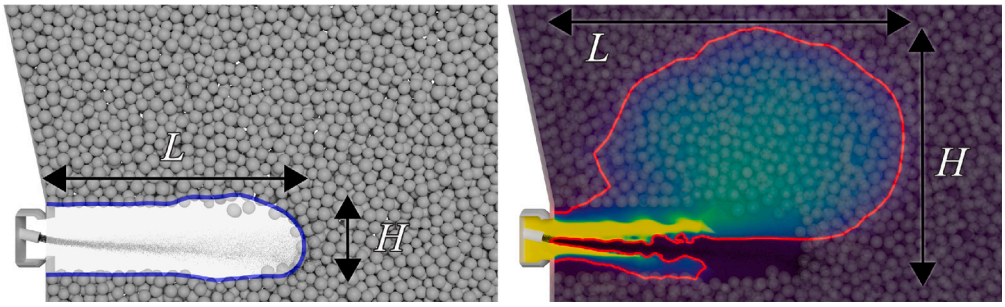

(a) Physical raceway (b) Chemical raceway

Fig. 1. Illustration of the physical and chemical raceway definition. (a) Physical raceway: the boundary of the physical raceway is outlined in blue. (b) Chemical raceway: the boundary of the chemical raceway is outlined in red. Coke particles are made transparent. The color map depicts the concentration of O_2 and the boundary is where the O_2 concentration falls below 5%.

(2,200 °C) and high pressure (4 bar), which make direct measurement nearly impossible. Numerical modeling has emerged as an effective tool for unraveling complex physics and chemistry, and providing insight into industrial-scale raceway studies.

Over the years, both experimental and numerical studies have investigated raceway phenomena in a *cold* environment, wherein chemical reactions and heat transfer were not taken into consideration (Umekage et al., 2006; Wright et al., 2011; Hilton and Cleary, 2012; Rangarajan et al., 2014; Hou et al., 2016; Miao et al., 2017; Rabadan Santana et al., 2019). With the advancement of computer processing units, there has been a shift towards studying the raceway phenomena in a *hot* environment. Starting in the early 2010s, Shen et al. provided the first understanding of PC combustion in a raceway and its behavior under various operating conditions by numerical models (Shen et al., 2011, 2012, 2014; Shen and Yu, 2015). Despite this breakthrough, the shape and size of the raceway were considered stagnant in the models due to the limitation of computational capacity. In the early 2020s, the dynamic raceway was adopted in several studies. Zhuo et al. developed a sophisticated raceway model using TFM on the gas-coke interaction while treating pulverized coal as Lagrangian points (Zhuo and Shen, 2020). Their model described a dynamic evolution of raceway and the combustion of pulverized coal. However, the interaction of coke and coal is not considered, and the combustion of the volatile matter was limited to the Eddy Dissipation Model. Cui et al. simulated an industrial-scale raceway, taking into account coke oxidation using the reactive CFD-DEM method (Cui et al., 2020). Xu et al. further advanced the study by introducing coarse-grained coke particles with a scaling factor of 2 (Xu et al., 2022); nevertheless, pulverized coal was not considered in the model. To the best of our knowledge, no hot raceway model has been developed that takes into account the concurrent dynamics of both coke and PC using the DEM and incorporates gas phase reactions through a well-established combustion mechanism. On the one hand, the simultaneous consideration of coke and PC dynamics enables the prediction of PC trajectories within the coke channels and the possible resultant formation of the bird's nest; on the other hand, the incorporation of a comprehensive combustion mechanism results in a more accurate prediction of raceway thermodynamics.

In this work, we develop a transient CFD-DEM (Discrete Element Method) model that simulates the coke and PC as soft-sphere particles and considers the combustion of volatile matter as a non-premixed flame. The DEM can describe not only the dynamics of the coke bed and PC but also their interaction. The Flamelet Generated Manifold (FGM) method (Van Oijen et al., 2001) is employed to model the pulverized coal flame with the benefit of reducing the computational cost of the complex combustion chemistry by looking up the combustion status from a pre-computed database. Additionally, a coarse-graining method (Benyahia and Janine, 2010; Radl et al., 2011) is applied to the PC particles to ease the computational burden further. These reduction techniques make the industrial-scale CFD-DEM model for comprehensive raceway combustion modeling feasible while not compromising accuracy.

In this paper, we first present the numerical methods that formulate the CFD-DEM model. It is followed by the description of the simulation setup and the boundary and initial conditions. The results section begins with the definitions of the physical and chemical raceway, as illustrated in Fig. 1, and shows their evolution for a base case. We then analyze the dynamics and utilization of pulverized coal to evaluate the performance of the simulated BF tuyere. Subsequently, we examine the impact of varying operating conditions, including pulverized coal injection (PCI) rate and the lance angle for PC transport. We identify the factors responsible for the formation of the physical and chemical raceway. Finally, the utilization of PC under diverse lance configurations is demonstrated. This study concludes with a summary of key findings and future outlooks.

2. Numerical methods

This section provides a summary of the applied CFD-DEM model, which incorporates the Coarse-Graining and Flamelet Generated Manifold (FGM) method. The model was developed within the framework of a combination of several open-source toolboxes: OpenFOAM® (Weller et al., 1998) for CFD and FGM, LIGGGHTS® (Kloss et al., 2012) for DEM, and CFDEM® (Kloss et al., 2012) for the multiphase coupling, including momentum, heat, and mass transfer. This model has been validated with a well-defined small-scale experimental study of pulverized coal combustion, which was presented in our previous publication (Huang et al., 2022). For simplicity of current paper, we outline the governing equations in Table 1 and elaborate only on the additional features used in the present simulations.

2.1. Discrete phase

2.1.1. Particle mass balance

Both pulverized coal and coke undergo gasification, a process in which solid fuel coal is converted into chemically reactive gases (Ishii, 2000). However, the sub-processes involved in the gasification of pulverized coal and coke are different. Pulverized coal contains volatile matter that is released during heating until it is depleted, a process known as devolatilization, Eq. (14). After this, the remaining char is converted to the gas phase by oxidizers, a process called char conversion, Eq. (15). In contrast, since coke does not contain much volatile matter, it only undergoes char conversion during gasification. Note that in reality, these sub-processes occur sequentially with some overlapping in time. In this study, the gasification is simplified into two sequential processes, first devolatilization (if applicable) and then char conversion. The compositions of coke and pulverized coal are given in Table 2.

Table 1
Governing equations for gas phase, solid phase, and multiphase coupling (Huang et al., 2022).

Name	Equations	
Gas phase		
continuity	$\frac{\partial(\epsilon\bar{\rho}_f)}{\partial t}+\frac{\partial(\epsilon\bar{\rho}_f\tilde{u}_j)}{\partial x_j}=S_p$	(1)
momentum	$\frac{\partial(\epsilon\bar{\rho}_f\tilde{u}_i)}{\partial t}+\frac{\partial(\epsilon\bar{\rho}_f\tilde{u}_i\tilde{u}_j)}{\partial x_j}=-\epsilon\frac{\partial\bar{p}}{\partial x_i}+2\epsilon\frac{\partial}{\partial x_i}\left[\mu_{\text{eff}}\left(\tilde{S}_{ij}-\frac{1}{3}\tilde{S}_{kk}\delta_{ij}\right)\right]-\frac{1}{V_{\text{cell}}}\sum_{n=1}^{n_p}\vec{f}_D^{\,n}+\epsilon\bar{\rho}_f\vec{g}$	(2)
Z_{devol}	$\frac{\partial\epsilon\bar{\rho}_f\widetilde{Z}_{\text{devol}}}{\partial t}+\frac{\partial\epsilon\bar{\rho}_f u_i\widetilde{Z}_{\text{devol}}}{\partial x_i}=\epsilon\frac{\partial}{\partial x_i}\left[\left(\frac{\mu}{\text{Sc}}+\frac{\mu_t}{\text{Sc}_t}\right)\frac{\partial\widetilde{Z}_{\text{devol}}}{\partial x_i}\right]+\widetilde{S}_{\text{devol}}$	(3)
Z_{char}	$\frac{\partial\epsilon\bar{\rho}_f\widetilde{Z}_{\text{char}}}{\partial t}+\frac{\partial\epsilon\bar{\rho}_f u_i\widetilde{Z}_{\text{char}}}{\partial x_i}=\epsilon\frac{\partial}{\partial x_i}\left[\left(\frac{\mu}{\text{Sc}}+\frac{\mu_t}{\text{Sc}_t}\right)\frac{\partial\widetilde{Z}_{\text{char}}}{\partial x_i}\right]+\widetilde{S}_{\text{char}}$	(4)
progress variable	$\frac{\partial\epsilon\bar{\rho}_f\widetilde{Y}_{\text{PV}}}{\partial t}+\frac{\partial\epsilon\bar{\rho}_f u_i\widetilde{Y}_{\text{PV}}}{\partial x_i}=\epsilon\frac{\partial}{\partial x_i}\left[\left(\frac{\mu}{\text{Sc}}+\frac{\mu_t}{\text{Sc}_t}\right)\frac{\partial\widetilde{Y}_{\text{PV}}}{\partial x_i}\right]+\widetilde{\dot{\omega}}_{PV}$	(5)
enthalpy	$\frac{\partial\epsilon\bar{\rho}_f\widetilde{H}}{\partial t}+\frac{\partial\epsilon\bar{\rho}_f u_i\widetilde{H}}{\partial x_i}=\epsilon\frac{\partial}{\partial x_i}\left[\left(\alpha_f+\frac{\mu_t}{\text{Pr}_t}\right)\frac{\partial\widetilde{H}}{\partial x_i}\right]-\frac{1}{V_{\text{cell}}}\sum_{n=1}^{n_p}\left[Q_{n,\text{conv}}+Q_{n,\text{rad}}+\frac{dm_{n,\text{devol}}}{dt}h_{\text{devol}}+\frac{dm_{n,\text{char}}}{dt}h_{\text{char}}+\frac{dm_{n,Boud}}{dt}h_{Boud}\right]$	(6)
Solid phase (coke and pulverized coal)		
momentum	$m_p\frac{d\vec{u}}{dt}=m_p\vec{g}+\vec{f}_D+\vec{f}_C$	(7)
angular momentum	$I_p\frac{d\vec{\omega}}{dt}=\vec{T}_T+\vec{T}_r$	(8)
mass	$\frac{dm_p}{dt}=\frac{dm_{\text{VM},p}}{dt}+\frac{dm_{\text{char},p}}{dt}+\frac{dm_{Boud,p}}{dt}$	(9)
energy	$m_pC_{p,p}\frac{dT_p}{dt}=Q_{\text{conv}}+Q_{\text{devol}}+Q_{\text{char}}+Q_{\text{Boud}}+Q_{\text{rad}}$	(10)
Multiphase coupling		
drag (Beetstra et al., 2007)	$\vec{f}_D=3\pi\mu_{\text{eff}}\epsilon d_p\lvert\vec{u}-\vec{v}\rvert\left\{\frac{10(1-\epsilon)}{\epsilon^2}+\epsilon^2\left(1+1.5\sqrt{(1-\epsilon)}\right)+\text{Re}_p\left[\frac{0.413}{24\epsilon^2}\frac{\epsilon^{-1}+3\epsilon(1-\epsilon)+8.4\text{Re}_p^{-0.343}}{1+10^{3(1-\epsilon)}\text{Re}_p^{-(1+4\epsilon)/2}}\right]\right\}$	(11)
convection	$Q_{\text{conv}}=\frac{N\tilde{u}\lambda_f}{d_p}A_p\left(T_f-T_p\right)$	(12)
radiation	$Q_{\text{rad}}=e_p\left(\frac{G}{4}-\sigma T_p^4\right)A_p$	(13)

Table 2
Compositions of pulverized coal and coke.

	Pulverized coal	Coke
Volatile matter	43.58 wt.%	0 wt.%
CH_4	55 wt.%	-
C_2H_2	11 wt.%	-
CO	34 wt.%	-
Char	56.42 wt.%	100 wt.%
C	100 wt.%	100 wt.%

Table 3
Coefficients for estimating particle specific heat in Eq. (18).

Coefficient c_i	Value
c_0	1080
c_1	3.81
c_2	5.48×10^{-4}
c_3	-7.83×10^{-5}
c_4	3.99×10^{-9}

devolatilization: $\text{PC}\rightarrow\text{VM}+\text{C}$ (14)

char oxidation: $\text{C}+\frac{1}{2}\text{O}_2\rightarrow\text{CO}$ (15)

Boudouard reaction: $\text{C}+\text{CO}_2\rightarrow2\text{CO}$ (16)

The process of devolatilization is simulated using the Single First Order Reaction model proposed by Badzioch and Hawksley (1970). The char oxidation is modeled using the approach introduced by Baum and Street (1971). In this study, it is assumed that during devolatilization the loss of particle mass does not cause changes in particle size, and hence only the solid density decreases. However, during char oxidation, the loss of char mass results in a size reduction, while maintaining a constant density. Further details are discussed in our previous work (Huang et al., 2022).

The Boudouard reaction, which was not included in our previous work, is introduced to account for the heterogeneous reaction of CO_2 on particles (Eq. (16)). It is necessary to include this reaction as at temperatures above 1,000 °C, all CO_2 is converted into CO if in contact with coke particles (Geerdes et al., 2020). The Boudouard reaction is described by the Langmuir-Hinshelwood mechanism (Kashiwaya and Ishii, 1991):

$$\frac{dm_{Boud,p}}{dt}=-\frac{\left(k_{1,c}C_{c,0}+k_{1,a}C_{a,0}\right)P_{CO_2}}{1+k_2P_{CO}+k_3P_{CO_2}}m_{char} \tag{17}$$

where P_{CO_2} and P_{CO} are the partial pressures of CO_2 and CO, respectively, and $k_{1,c}$, $k_{1,a}$, $C_{c,0}$, $C_{a,0}$, k_2, and k_3 are the model parameters that are taken from the work of Kashiwaya and Ishii (1991).

2.1.2. Particle heat capacity

The specific heat capacity of coke and PC increases with rising temperature. To account for the effect of temperature, the particle heat capacity is estimated using Merrick's model (Merrick, 1983),

$$c_p=\sum_{i=0}^{4}c_iT_p^i \tag{18}$$

where the coefficients c_i provided by Tomeczek and Palugniok (1996) are used, as shown in Table 3. The specific heat is capped at 2,500 J/(kg K) to prevent numerical instability when the temperature rises above 1,585 °C. In this study, it is assumed that Eq. (18) is applicable on both coke and PC.

2.2. Continuum phase

2.2.1. Species transport

The standard FGM approach solves the transport equation of a progress variable and mixture fractions. The species mass fractions are then retrieved from the database. To improve the accuracy of important

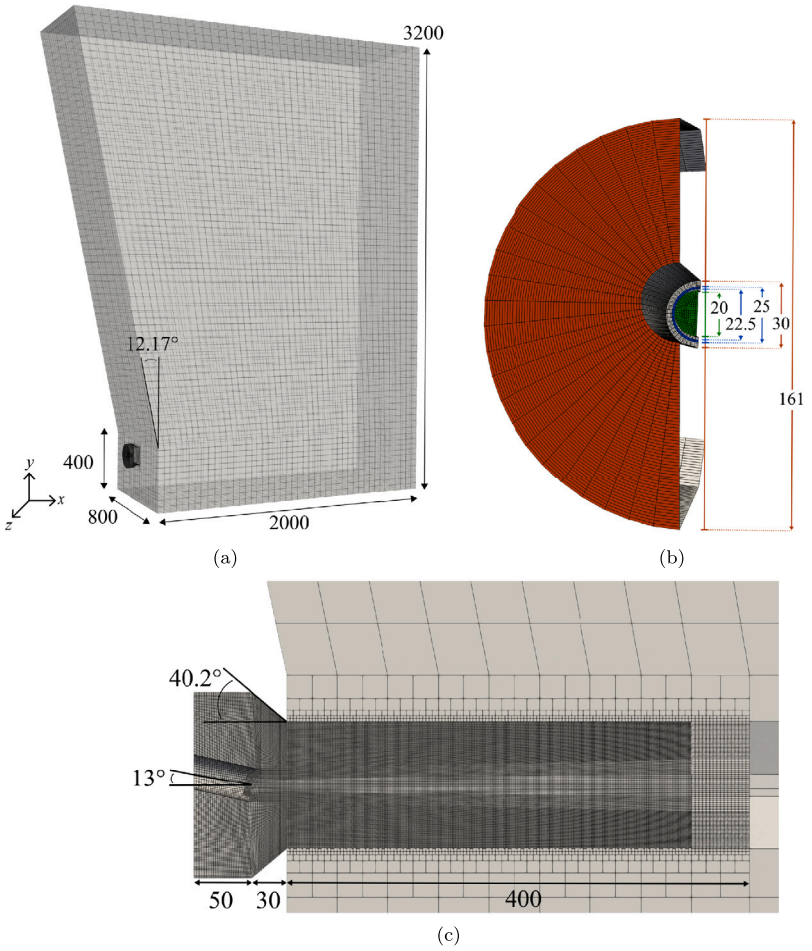

Fig. 2. Geometry and dimensions of the simulation grid. All units are in millimeters. (a) Computational domain constructed by a total of 1.4 million cells. (b) Surface with cell edges of injection pipe, cooling gas, and lance. (c) Cross section of the injection zone.

species, i.e. O_2, CO, and CO_2, additional transport equations are solved, Eqs. (19) to (21).

$$\frac{\partial \varepsilon \bar{\rho}_f \widetilde{Y}_{O_2}}{\partial t} + \frac{\partial \varepsilon \bar{\rho}_f u_i \widetilde{Y}_{O_2}}{\partial x_i} = \varepsilon \frac{\partial}{\partial x_i}\left[\left(\frac{\mu}{\mathrm{Sc}} + \frac{\mu_t}{\mathrm{Sc}_t}\right)\frac{\partial \widetilde{Y}_{O_2}}{\partial x_i}\right] + \widetilde{\omega}_{O_2} \tag{19}$$

$$\frac{\partial \varepsilon \bar{\rho}_f \widetilde{Y}_{CO}}{\partial t} + \frac{\partial \varepsilon \bar{\rho}_f u_i \widetilde{Y}_{CO}}{\partial x_i} = \varepsilon \frac{\partial}{\partial x_i}\left[\left(\frac{\mu}{\mathrm{Sc}} + \frac{\mu_t}{\mathrm{Sc}_t}\right)\frac{\partial \widetilde{Y}_{CO}}{\partial x_i}\right] + \widetilde{\omega}_{CO} \tag{20}$$

$$\frac{\partial \varepsilon \bar{\rho}_f \widetilde{Y}_{CO_2}}{\partial t} + \frac{\partial \varepsilon \bar{\rho}_f u_i \widetilde{Y}_{CO_2}}{\partial x_i} = \varepsilon \frac{\partial}{\partial x_i}\left[\left(\frac{\mu}{\mathrm{Sc}} + \frac{\mu_t}{\mathrm{Sc}_t}\right)\frac{\partial \widetilde{Y}_{CO_2}}{\partial x_i}\right] + \widetilde{\omega}_{CO_2} \tag{21}$$

The source term $\widetilde{\omega}_{O_2}$ includes the consumption due to gas combustion and is calculated from the heterogeneous reaction Eq. (15). $\widetilde{\omega}_{CO}$ includes the release from the devolatilization process, the source/sink due to gas combustion, and the production from heterogeneous reactions Eqs. (15) and (16). $\widetilde{\omega}_{CO_2}$ includes the source/sink gas due to combustion and the consumption from the heterogeneous reaction Eq. (16). Other species, i.e. N_2, H_2O, or H_2, are retrieved directly from the FGM database.

2.2.2. Flamelets model

To construct the FGM look-up database, a collection of one-dimensional non-premixed flamelets are generated using Chem1d (Somers, 1994) with the GRI-MECH 3.0 mechanism (Smith et al., 1999), which contains 325 reactions and 53 species. Each flamelet is calculated at a certain mixture fraction ratio X and a certain boundary temperature T_b at a pressure of 4 bar. The definition of X can be found in our previous study (Huang et al., 2022). The parameters X and T_b vary from 0 to 1 and from 300 K to 1,500 K, respectively. For each value of X and T_b, a steady-state solution is acquired with the strain rate from 10 to the extinction limit. After the extinction limit has been reached, a transient simulation is conducted to capture the quenching behavior.

3. Simulation setup

3.1. Geometry

The computational grid and geometry for the raceway model are shown in Fig. 2, the choice of which are based on the input from the industrial partner. Typically, a commercial blast furnace consists of a number of tuyeres. However, to limit the computation cost to an affordable level, only a slice of the BF containing one tuyere in an injection zone is considered. The reference case has a lance angle pointing slightly downward at −13° relative to the horizontal x-z plane. Another two lance angles (0° and +13°) will be used to examine their effect on raceway phenomena. In both cases, the grid cells' location and orientation change according to the lance angle while the total number of cells remains the same. In Fig. 2b, the boundary patches are labeled in different colors: red for the hot blast, blue for the cooling gas, and green for the carrying gas. All other boundaries are considered walls except for the outlet patch at the top of the domain.

3.2. Boundary and initial conditions

Table 4 lists the boundary and initial conditions for the gas and solid phases. The high-speed air inlet velocity is set to 80 m/s or 96 m/s,

Table 4
Boundary and initial conditions.

Conditions		Values	Conditions		Values
Boundaries			Particles		
Blast speed[1]	(m/s)	200, 240	Coke temperature	(K)	1300
Blast O_2 content	(wt.%)	37.0	Coke particle size	(mm)	Fig. 3a
Blast temp.	(K)	1000	Coke density	(kg/m^3)	800
Cooling gas velocity	(m/s)	30	Coke heat capacity	(J/(kg K))	Eq. (18)
Cooling gas temp.	(K)	300	PC injection temp.	(K)	600
Carrying gas velocity[2]	(m/s)	30	PC particle size	(μm)	Fig. 3b
Carrying gas temp.	(K)	600	PC density	(kg/m^3)	1000
Outlet velocity	(m/s)	ZG[3]	PC injection rate	(kg/s)	0 - 0.6
Outlet pressure	(atm)	3.8	PC heat capacity	(J/(kg K))	Eq. (18)

[1] Blast speed refers to the air blast leaving the tuyere. The mean blast inlet velocity is set to 80 m/s and 96 m/s. Due to the contraction of the tuyere, air speed accelerates to 200 m/s and 240 m/s, respectively. The blast inlet is subjected to DFSEM for turbulence generation.
[2] Carrying gas is subjected to DFSEM for turbulence generation.
[3] Zero gradient.

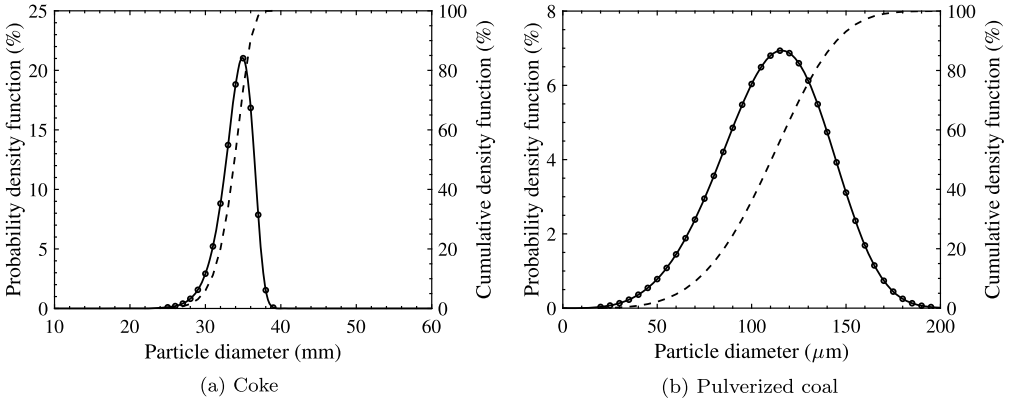

Fig. 3. Particle size distribution of (a) Coke and (b) Pulverized coal. The solid lines follow the Rosin-Rammler distribution with the scale and shape parameters of 35 and 20 for coke; 122.6 and 4.5 for pulverized coal. The mass-based and number-based mean diameters are 34.44 mm and 34.07 mm for coke; 130.0 μm and 111.8 μm for pulverized coal. The solid circles indicate the discrete sampling particle diameter. The dashed lines indicate the sampled cumulative density function.

Table 5
Particle interaction parameters used in DEM.

	Young's modulus	Poisson ratio	restitution coefficient	friction coefficient
pulverized coal	1×10^7 Pa	0.5	0.8	0.15
coke	2×10^7 Pa	0.5	0.8	0.15

yielding a blast volume of 3667 STP m^3/min or 4400 STP m^3/min, respectively, if considering a total of 32 tuyeres. Due to the contraction of the tuyere, these injection velocities correspond to an average speed of 200 m/s and 240 m/s, respectively, at the exit of the tuyere. The accelerated air speed is termed blast speed in this study. The Divergence-Free Synthetic Eddy Method (DFSEM) (Poletto et al., 2013) is used to generate the inflow turbulence at the patch of the blast air and the lance (orange and green patch in Fig. 2b, respectively). The pulverized coal flame is ignited by delivering volatile matter at the stochiometric condition via the pilot (blue patch in Fig. 2b) for the first 2 ms. After this time period, the pilot port is closed, resulting in no gas outflows. The outlet pressure is prescribed with a pressure of 3.8 bar, which allows the pressure to build up to 4 bar at the tuyere. The furnace walls exhibit a no-slip condition and have collision and friction with both coke and PC particles.

Coke particles typically have a harmonic mean diameter of 50 mm when charged from the top of the furnace. Due to gasification and abrasion during descent, the particle harmonic mean diameter drops to around 35 mm at the level of injection (Geerdes et al., 2020). As a result, the coke particle size used in simulations follows a Rosin-Rammler particle size distribution with a scale parameter of 35 and a shape parameter of 25, giving a mass-based mean diameter of 34.44 mm and a number-based mean diameter of 34.07 mm, as shown in Fig. 3a. This distribution is rather narrow in order to avoid too many small coke particles being simulated and compromising the simulation time. In total, 145,000 coke particles are present in the domain, giving an initial packing height of 2.8 m. It has been tested that including more coke particles does not alter the shape and size of the physical raceway. As for interactions between particles, a single set of collisional parameters as shown in Table 5 is used.

The unresolved CFD-DEM method used in this study requires particle size to be smaller than the grid size.[1] Otherwise, simulations will suffer from instability and inaccuracy. This conflicts with the need for a fine grid near the tuyere. Therefore, a permeable wall is placed in front of the tuyere and extended into the furnace to prevent coke particles from falling into the fine mesh region. However, this permeable wall placement can be considered as an extrusion of the tuyere and its length can affect the raceway penetration length (Miao et al., 2017). To preserve the fine mesh region for resolving the combustion and turbulence

[1] Three levels of mesh, coarse (0.6M cells), medium (1.2M cells), and fine (1.8M cells) meshes were tested. The medium mesh leads to converging results similar to the fine mesh.

while at the same time not extending the raceway length by elongating the wall, a permeable wall with a length of 0.4 m and a height and width of 0.2 m is finally used in this study after careful assessment. An alternative approach is to use the dual-grid method (Deb and Tafti, 2013; Farzaneh et al., 2011; Pozzetti et al., 2018), which solves the fluid governing equations on a fine mesh and couples the multiphase transport on a coarse mesh, thus eliminating the need for a permeable wall.

The simulations involve the use of coarse-grained PC parcels, with each parcel being 8 times larger than the primary particle[2] and representing 8^3 primary particles that have identical size and physical characteristics. It is important to note that throughout this study, the results regarding PC size have been interpreted in terms of the size of primary particles, unless explicitly stated otherwise. The PC particles possess a Rosin-Rammler size distribution, with a scale parameter of 122.6 and a shape parameter of 4.5. This yields a mass-based mean diameter of 130.0 μm and a number-based mean diameter of 111.8 μm (the size of coarse-grained parcels being 8 times larger), as illustrated in Fig. 3b. The injection process positions the PC parcels within a 2 mm reserved region in the lance, where their velocities are interpolated from the CFD cells in which they reside. This approach assumes that the PC parcels have reached their terminal velocities during transport.

PC particles are removed from the simulation when their size is smaller than 2 μm or their residence time is longer than 20 ms. Before these particles are removed, they mainly remain in the coke bed, where oxygen is scarce and their volatile matter has been depleted. As a result, they contribute little to gas phase combustion or gasification. Removing them from the simulation not only prevents the accumulation of PC particles from hampering the computation but also does not significantly impact the overall simulation results.

3.3. Simulation procedure

The initial coke bed for the simulations is prepared by free-falling coke particles from the top and settling under the influence of gravity. Pulverized coal is then injected via the lance, and blast air is introduced through the blast pipe. The initial O_2 content of the bed is 37 wt.%, which is the same as in the blast. By initializing the bed with O_2, the coke oxidation reaction (Eq. (15)) occurs rapidly at the outset, providing sufficient thrust to lift the bed temporarily, as will be discussed in Section 4. This approach enables the coke bed to loosen the packing of coke particles that may have formed during the free-falling process. Furthermore, it allows the raceway to enter the hysteresis regime, as observed in the experiment (Gupta et al., 2005), without the need to gradually increase and then decrease the blast velocity to reach the desired velocity.

The computation was carried out on the Dutch National Supercomputer Snellius. Each simulation utilized 128 cores in parallel on two AMD Rome 7H12 CPUs with a clock frequency of 2.6 GHz and 2 GiB of memory per core. The simulations started from their initial conditions until a physical runtime of 1.0 seconds, where a pseudo steady state was observed.

4. Results

4.1. Physical and chemical raceway

The physical raceway is the void region bounded by coke particles, as illustrated in Fig. 1a. We define the boundary of a physical raceway at the location where the void fraction intersects a threshold of 0.8. The length of the physical raceway is measured horizontally from the end of the tuyere until the iso-surface, the height is measured vertically from the lowest point to the highest point of the iso-surface, and the width is measured horizontally from front to back of the iso-surface.

Unlike the physical raceway, the chemical raceway has not been the focus of raceway modeling studies. No common definition of the chemical raceway has been established so far. Nishi et al. defined the boundary of a chemical raceway at the location where temperature changes abruptly (Nishi et al., 1982) whereas Atkinson and Willmers defined it as the location where the CO_2 level falls below 2% (Atkinson and Willmers, 1990). We argue that these definitions are not suitable. Firstly, the gas temperature peaks at the location of the pulverized coal flame. Thus, the location of abrupt temperature change mainly encloses the region where pulverized coal combustion takes place. Secondly, CO_2 is produced from the gas phase combustion and consumed by the Boudouard reaction. Its concentration rises above or falls below the threshold (Jamaluddin, 1985), making the boundary spatially discontinuous.

As a result, we propose that the boundary of the chemical raceway can be defined at the location where the O_2 mass fraction falls below a threshold of 5%, as illustrated in Fig. 1b. O_2 is consumed by the pulverized coal flame (gas phase combustion) as well as by char oxidation. Its concentration can only decrease, and the boundary is smoother than that defined by the CO_2, making the analysis easier.

Fig. 4 shows the qualitative evolution of the physical raceway while Fig. 5 depicts the quantitative evolution of the physical and chemical raceway from the base case, where the pulverized coal injection (PCI) rate is set at 0.4 kg/s and the blast speed is 200 m/s. It can be observed that the physical raceway undergoes growth and contraction, eventually attaining a stable form after the first half second. The initial growth of the physical raceway is attributed to the outgassing of CO. At the outset, the coke bed is filled with 37 wt.% of O_2, and the coke has a temperature of 1,300 K. Thus, the char oxidation releases enough CO to lift the coke bed temporarily, which creates a pathway for the blast air and consequently forms a physical raceway. Note that in reality there is only CO and no O_2 in the shaft, so this can be considered as a simulation artifact. As the O_2 in the bed is depleted, the raceway quickly contracts to a stable size due to the heavy burden above. Note that the physical raceway resembles a balloon shape during the period of CO outgassing and collapses to an elongated shape when stabilized. The height and width of the physical raceway both stabilize at 0.2 m, as a consequence of the presence of the permeable wall that has the same height and width.

On the other hand, the chemical raceway starts larger in size due to the initial rich O_2 condition and quickly contracts due to the fast consumption of O_2 from coke oxidation. When comparing the physical and chemical raceway sizes, it can be seen that the chemical raceway is larger in length, height, and width than its physical counterpart. The difference can be attributed to the permeation of O_2 into the coke bed, allowing for char oxidation to occur. This finding indicates that not all crucial reactions occur solely within the confinement of the physical raceway for this geometric setup.

Finally, Fig. 6 displays the cross-sectional distributions of O_2 and CO at pseudo steady state (at 1 s). The O_2 in the stream of the blasted air is rapidly consumed through the combustion of volatile matter released from the devolatilization of PC and the oxidation with PC char. This results in low O_2 content in areas where PC is present. The remaining O_2 travels into the coke bed to react with the coke. From Fig. 6b, it can be observed that a stream of CO is produced at the location where O_2 is depleted. The production of CO originates from the devolatilization, the product of volatile matter combustion, and char oxidation. This stream of CO is not further oxidized into CO_2 due to the lack of O_2 downstream. It can be seen that the CO stream travels in the direction of the PC jet and is redirected upward by the end of the domain, although in reality, this may not occur as the coke bed is permeable and the CO stream can travel further in the radial direction. However, in the simulations, the end of the computation domain is treated as a wall, mimicking a dense dead man.

[2] Four coarse-graining factors, 4, 6, 8, 10, were tested and with a factor of 8 the simulation still produces converging results.

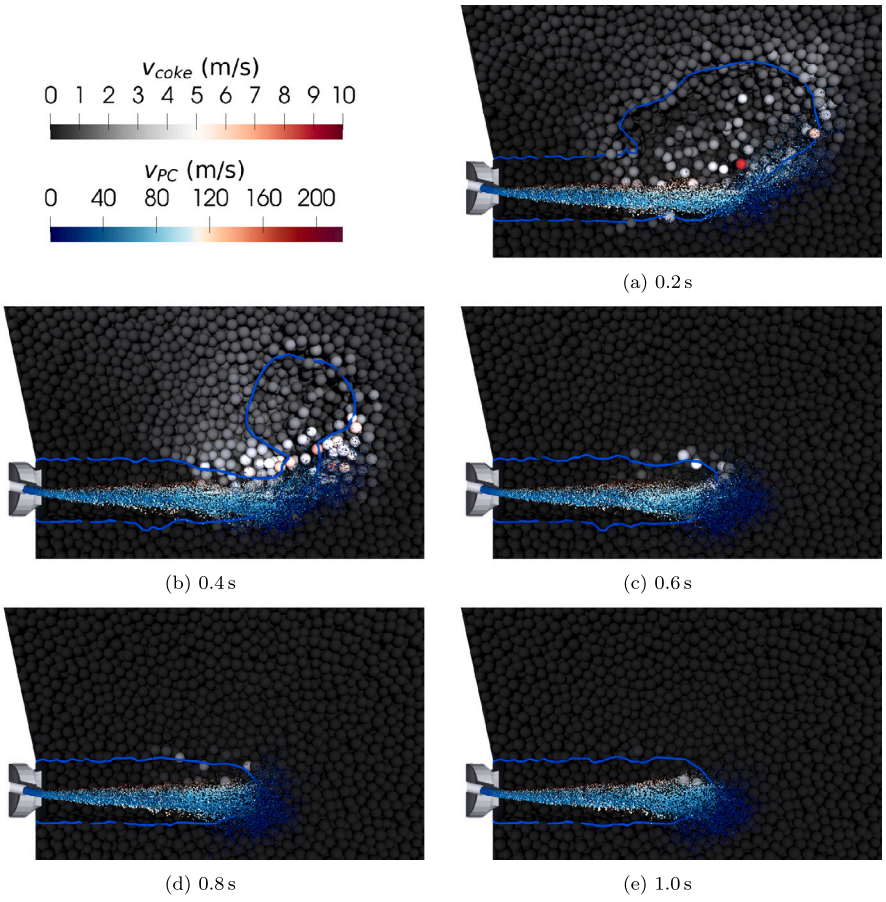

Fig. 4. A series of snapshots displays the evolution of the physical raceway over time. Each snapshot features a blue contour indicating the boundary of the physical raceway, drawn at the location where the void fraction is 0.8 on the x-y plane. The velocities of coke and pulverized coal (PC) are shown using different color maps. PC parcels are enlarged by a factor of 5 to aid visualization. The coke bed is shown clipped in half in each snapshot.

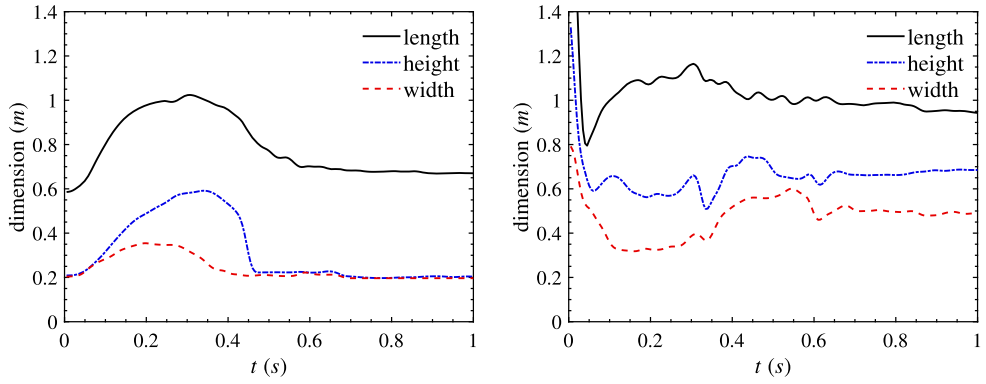

Fig. 5. Evolution of physical and chemical raceway dimension. Simulation conditions can be found in Table 4. The blast speed is 200 m/s and the PC injection rate is 0.4 kg/s. (a) Physical raceway (b) Chemical raceway.

4.2. Pulverized coal utilization

The particle size distribution of the PC plume is shown in Fig. 7a at six lateral positions x. A crescent shape of the particles' spatial distribution can be observed as the PC jet travels in the physical raceway. The formation of this crescent distribution is caused by the "bluff-body effect" (Majeski et al., 2015), which occurs when the blast air interacts with the lance creating a wake that can facilitate coal dispersion. Furthermore, the bluff-body effect also segregates PC particles of different sizes. Larger particles tend to stay at the bottom of the crescent, while smaller particles tend to stay at the tips of the crescent. The particle size segregation was also observed in the study of Wu et al. (2018). At the end of the physical raceway, the PC particles encounter the coke bed and disperse into coke channels, as shown in the bottom-right subfigure.

Fig. 7b presents the burnout distribution of the PC plume at six lateral positions, where the devolatilization and char conversion processes are distinguished by two separate color maps. Burnout of individual particles is defined as the utilization in terms of mass loss from devolatilization and char conversion:

$$\text{burnout} = 1 - \frac{m_p}{m_{p,0}} \tag{22}$$

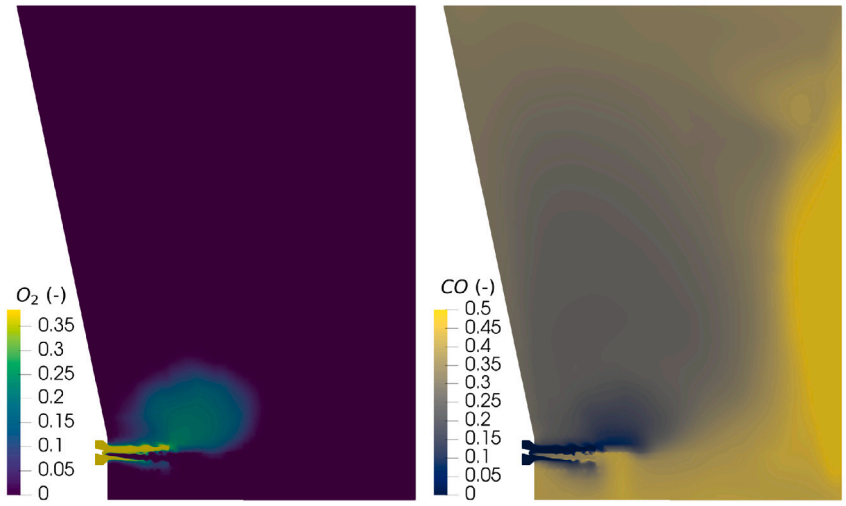

(a) O_2 (b) CO

Fig. 6. Cross-sectional snapshots of O_2 and CO mass fraction at pseudo steady state (captured at 1 s).

where m_p and $m_{p,0}$ are the particle mass and initial particle mass, respectively. It can be seen that all PC particles reach complete devolatilization at $0.5 < x < 0.6$ m, corresponding to approximately 10 ms of traveling time from the lance tip. At the end of the PC plume, only a few particles achieve complete burnout. When viewed together with Fig. 7a, it can be observed that the degree of burnout correlates to particle size. The quantitative results in Fig. 8a and Fig. 8b, which respectively display the trajectory and burnout for different particle size groups, evidently shows that, as expected, smaller particles burn out faster than larger particles. This is due to their faster heating rate through thermal convection with the surrounding flame, resulting in an earlier start of devolatization and a higher devolatilization rate. Once the volatile matter is depleted, the PC particles undergo char conversion, further increasing the burnout. As a result, some small particles reach 100% burnout in the downstream of the plume, leading to their removal from the simulations and consequently their average horizontal position y drops when $0.5 < x < 0.6$ m. In contrast, larger particles heat up more slowly, resulting in a slower devolatilization and lower burnout at the end of the plume. Furthermore, due to the bluff-body effect, large particles segregate to the bottom of the jet, where the O_2 content is almost entirely consumed. Their burnout after devolatilization increases only slightly compared to the smaller particles.

In Fig. 5a, the physical raceway length is shown to stabilize at $x = 0.67$ m. However, the trajectories of PC particles shown in Figs. 7a, 7b and 8 suggest that these particles can travel beyond this point ($x > 0.67$ m), and penetrate into the coke bed. As they travel through the coke channels, the particles experience a significant reduction in velocity and eventually accumulate close to the end of the physical raceway, potentially forming a low-permeability region, known as the bird's nest (Ishii, 2000). Fig. 9 illustrates the formation of such a bird's nest by accumulated pulverized coal particles over a period of 0.15 s. However, since pulverized coal only has a maximum allowed residence time of 20 ms in the simulations, it remains unclear how the long-term behavior of the bird's nest affects the gas flow and performance of pulverized coal burnout. Further investigations are necessary to fully understand the implications of the bird's nest.

4.3. Effect of pulverized coal injection rate

Existing raceway modeling studies in the literature have primarily focused on understanding the effects of varying blast velocities on the shape and size of the physical raceway without considering the combustion of pulverized coal due to computational limitations. From the current study, it is possible to determine if neglecting pulverized coal combustion is a reasonable assumption and hence, if previous studies can be considered valid. To this end, we compare the simulations with and without the pulverized coal injection (PCI). The simulation without PCI represents the case where only the momentum of the blast air contributes to the formation of the physical raceway, while the simulations with PCI (from 0.2 kg/s to 0.6 kg/s) represent the case where both the blast air and the combustion of the PC contribute to the formation of the physical raceway.

Figs. 10a and 10b presents the size of physical and chemical raceways for the blast speeds of 200 m/s and 240 m/s, respectively. For both blast speeds, the results indicate that the length and height of the physical raceway do not change with increasing PCI rates, confirming that pulverized coal combustion does not affect the size and shape of the physical raceway. This is due to the fact that the gas expansion resulting from the volatile flame is not strong enough to push the coke bed, and the momentum brought by the blast air alone is sufficient for physical raceway formation. Nevertheless, it should be noted that this conclusion is applicable only for a short time scale of 1 s. Heterogeneous combustion or abrasion-induced coke shrinkage in the proximity of the physical raceway may result in a reduced average coke particle size, resulting in lower resistance to physical raceway formation. However, the time scale for coke shrinkage is on the order of minutes, and its impact on the physical raceway is hence undetectable.

When comparing two blast speeds, it can be observed that 240 m/s yields a longer physical raceway and, generally, a larger chemical raceway as a result of higher blast momentum. The dimension of the chemical raceway is more susceptible to the PCI rate. In the absence of PCI, the chemical raceway size is determined by the char oxidation of coke. As the char oxidation rate of coke is relatively slow compared to pulverized coal, because of the surface reaction, the oxygen can permeate deeper into the coke bed. However, when PCI takes place, the oxygen consumption also involves pulverized coal combustion, leading to a significant reduction in the chemical raceway size. In general, the chemical raceway size slightly decreases with the increasing PCI rate, indicating more oxygen consumption. Nevertheless, the overall PC burnout drops with increasing PCI rate, as shown in Fig. 11. The overall PC burnout is calculated using

$$1 - \sum_{i}^{n_t} m_{p_i} / \sum_{i}^{n_t} m_{p_i,0} \tag{23}$$

where i indicates the index for the n_t particles that have the same residence time, including those particles that have been removed due to mass depletion. This calculation ensures the overall burnout considers

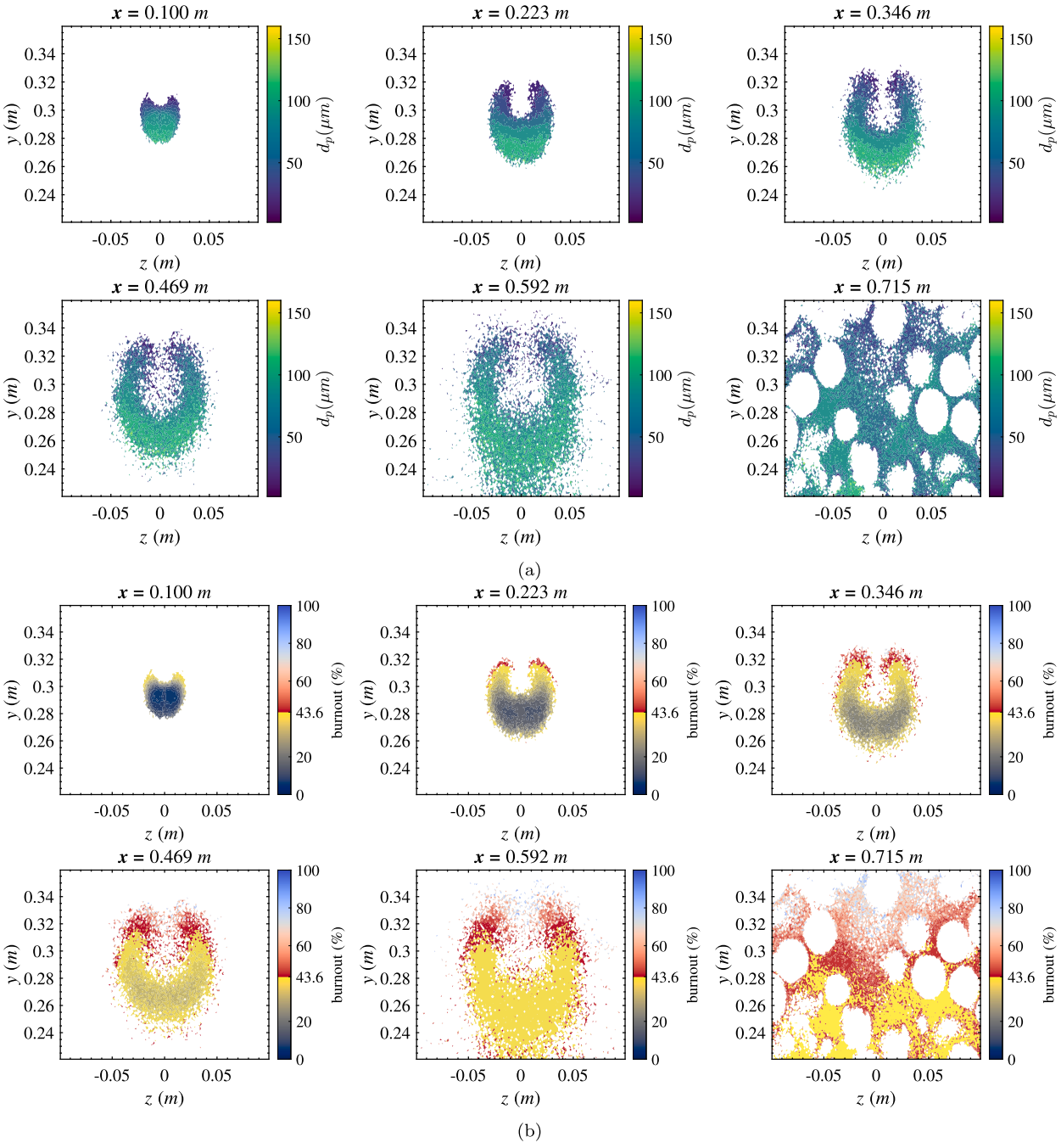

Fig. 7. Pulverized coal (a) particle size and (b) burnout distribution at different lateral positions x from upstream to downstream. The particle data is collected over time at a pseudo-steady state and then time-averaged. (a) The color labels particle size. In the last subfigure (bottom right), the white circular spots correspond to the presence of coke particles. (b) Two color maps are used to distinguish the devolatilization and char conversion processes. The color map switches at the devolatilization limit of 43.58%.

particles that are injected at the same time. The decrease in overall PC burnout with increasing PCI rate can be explained by the poor mixing of O_2 and PC. Fig. 12 shows the O_2 mass fraction and PC distribution at pseudo steady state for different PCI rates. It can be observed that the PC jet travels in a region lacking O_2 due to volatile matter combustion. Outside the volatile matter flame, abundant O_2 content is not mixed and reacted with PC but the O_2 instead enters the coke bed. Even with an increasing PCI rate (more PC particles), a similar amount of O_2 is used for char oxidation, resulting in decreased overall PC burnout.

This finding suggests that the mixing of O_2 and PC is important for the burnout of PC. To improve the hot blast-PC mixing, several injection systems have been applied in industries, including coaxial lances with O_2 flow in the outer pipe and coal flow in the inner pipe, special lance tip design to induce more turbulence, and the use of two lances at different entry angles (Geerdes et al., 2020). Ariyama et al. (1994) found that the double-lance configuration with one lance pointing slightly upward and the other pointing slightly downward can create two PC jets consuming different parts of the O_2 cloud, leading to better PC burnout compared to a single-lance configuration. In summary, our findings highlight the importance of proper mixing of oxygen and pulverized coal for efficient combustion. In order to improve the burnout of pulverized coal, future studies should continue focusing on designing configurations and methods that enhance the mixing of oxygen and pulverized coal.

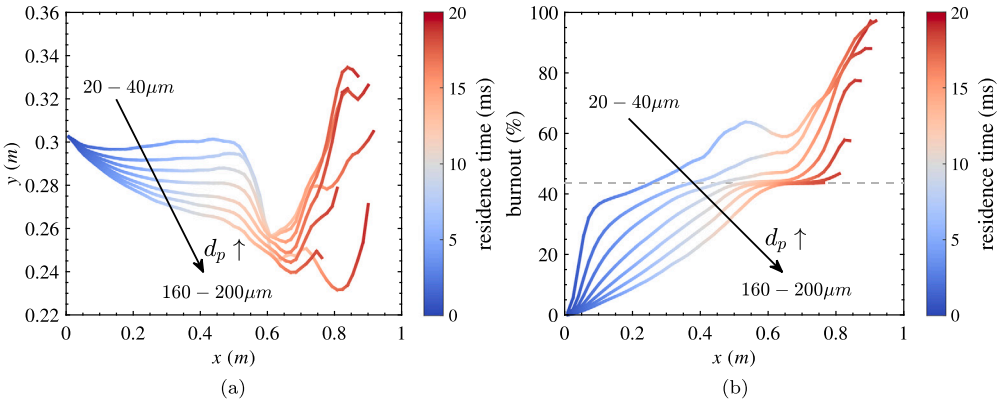

Fig. 8. (a) Trajectory and (b) burnout in different particle size groups, from 20-40 μm, 40-60 μm, 60-80 μm, 80-100 μm, 100-120 μm, 120-160 μm, and 160-200 μm. Each line displays information averaged within the corresponding particle size group. In (b), the gray dashed line indicates a complete devolatilization, which is at 43.58%.

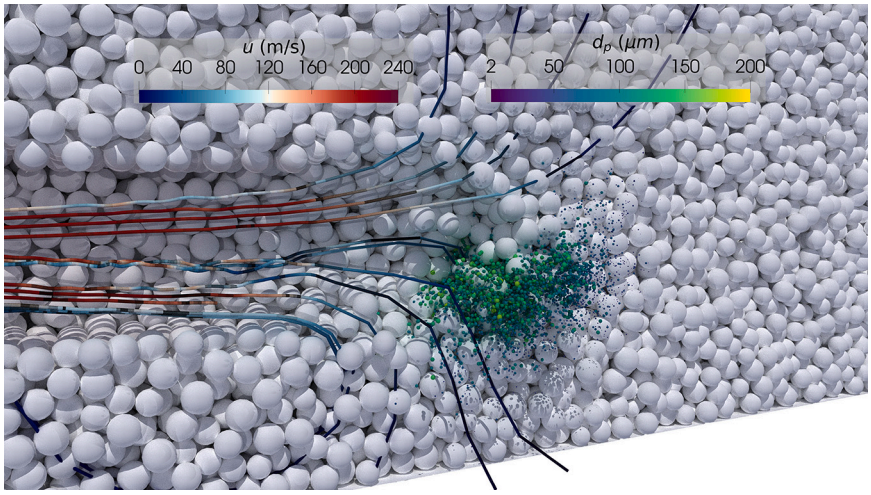

Fig. 9. Illustration of the formation of a bird's nest using pulverized coal data accumulated over a period of 0.15 s (from 0.85 s to 1.0 s) and coke and gas data captured at the exact time of 1.0 s. Only pulverized coal particles with a residence time of 20 ms (before they are removed from the simulation) are shown in the figure. The coke bed is clipped in half. The pulverized coal is color-coded according to particle size, while the coke is shown in white for better contrast. The streamlines are interpolated from the gas velocity. The size of pulverized coal parcels is enlarged 5 times for visualization.

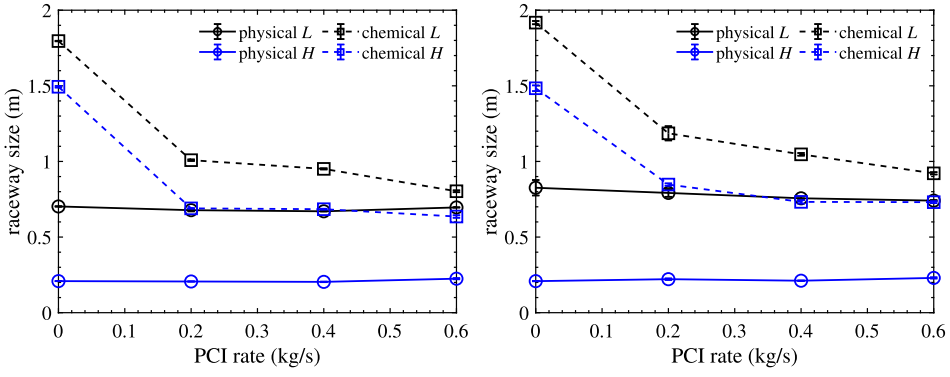

Fig. 10. Physical and chemical raceway size as a function of PCI rate. Only raceway length and height are shown for clarity. (a) blast speed 200 m/s. (b) blast speed 240 m/s.

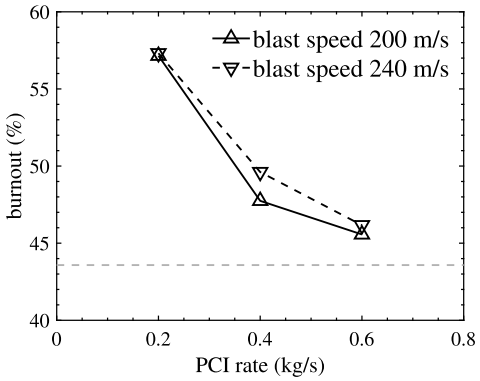

Fig. 11. Time-averaged overall PC burnout versus PCI rates. The gray dashed line indicates burnout contribution from the devolatilization (43.58%). In this graph, a residence time of 20 ms is used, and the overall PC burnout is averaged over a period of 0.15 s.

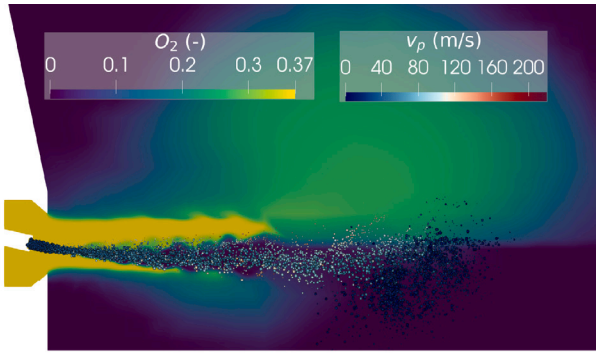

(a) PCI 0.2 kg/s

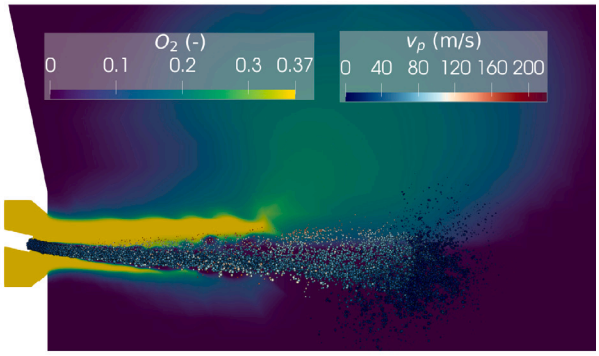

(b) PCI 0.4 kg/s

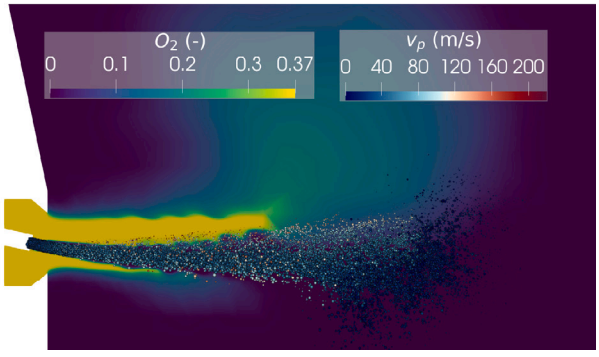

(c) PCI 0.6 kg/s

Fig. 12. Snapshots of PC jet and O_2 mass fraction at pseudo steady state. The pulverized coal parcel is enlarged 5 times for visualization.

4.4. Effect of lance angle

It was found that a significant amount of O_2 enters the coke bed without mixing or reacting with the PC, as shown in Fig. 6a. Intuitively, one would adjust the lance angle so that the PC jet can consume more O_2 content. Two different lance configurations were tested numerically: one with the lance placed horizontally and another with the lance directed upward at +13°. Fig. 13 shows snapshots of the O_2 and CO distributions at pseudo steady state. When the lance is placed horizontally, Fig. 13a shows that O_2 is consumed in the middle of the blast air, and the distribution of O_2 cloud in the coke bed is relatively symmetric. As the lance is placed slightly upward in +13°, Fig. 13b shows that the O_2 cloud in the coke bed mostly stays below the injection level. Comparing the three lance configurations, it can be observed that the position of the O_2 cloud is connected to the lance angle. Portions of O_2, if not in contact with the PC jet, can permeate into the coke bed and oxidize the coke.

Comparing the CO distribution from three lance configurations, Figs. 6b, 13c and 13d, it can be seen that the main difference lies in the path of CO. In the original configuration, the CO travels in the same direction as the PC jet until redirected upwards by the deadman. In the upper part of the domain, the CO is non-homogeneous due to the accumulation near the deadman. However, when the lance angle is increased to 0° and +13°, the CO in the upper part becomes more homogeneous, which can provide better conditions for the iron in the cohesive zone. However the cohesive zone is not taken into account in the current model. And note that in reality blast furnaces often have a larger radius than 5 m.

The performance of different lance configurations was quantitatively compared using PC utilization. The burnout in various particle size groups was shown in Fig. 14 for 0° and +13° lance configuration. The results showed that smaller particles burn out faster than larger ones, as we have seen in Fig. 8b, but there was no significant difference between the lance configurations. Except that the large particle groups in the 0° lance configuration burn out slower due to the absence of the bluff-body effect that promotes convective heat transfer induced by air-PC mixing. Despite this, complete devolatilization is achieved for all particle sizes. The overall burnout as a function of residence time was shown in Fig. 15. It can be seen that regardless of the lance angle, the PC burnout saturates at around 48% at the end of the PC lifetime, suggesting the consumption of O_2 by PC is not improved via changing the lance angle for this geometry. The profile from the 0° lance shows a slightly lower burnout rate due to, as mentioned, the lack of bluff-body effect.

5. Conclusions

A transient CFD-DEM model that describes the dynamics of raceways under the influence of pulverized coal (PC) combustion in an industrial-scale blast furnace is presented. This model can, for the first time, describe the dynamics of a raceway with the consideration of the interaction between PC and coke as well as the impact of gas combustion on the raceway. This model considers the lifetime of PC, including its injection, motion, thermochemical reactions, and interaction with the coke. Thanks to the model reduction via incorporating coarse-graining and FGM methods, raceway modeling at industrial scale is conducted with affordable computational cost by using high-performance computing.

The physical and chemical raceways are shown to differ in size and shape, suggesting that not all crucial reactions occur in the physical raceway, especially char oxidation. The PC jet exhibits a crescent-shaped spatial distribution, which is attributed to the bluff-body effect and results in particle size segregation within the jet. The utilization of PC is quantified in terms of burnout. It is shown that smaller PC particles generally undergo a higher degree of burnout as a result of faster convective heating and faster oxidation rate as compared to larger particles. Unburned PC particles penetrate into the coke bed at the end of

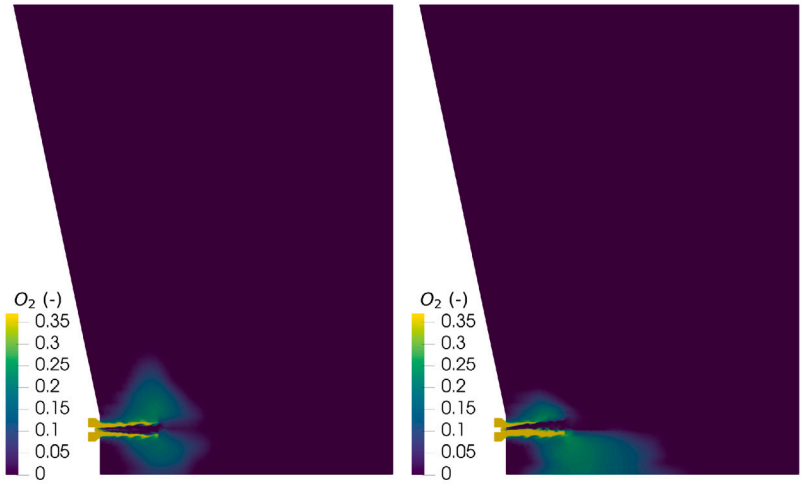

(a) O_2 0° lance configuration. (b) O_2 +13° lance configuration.

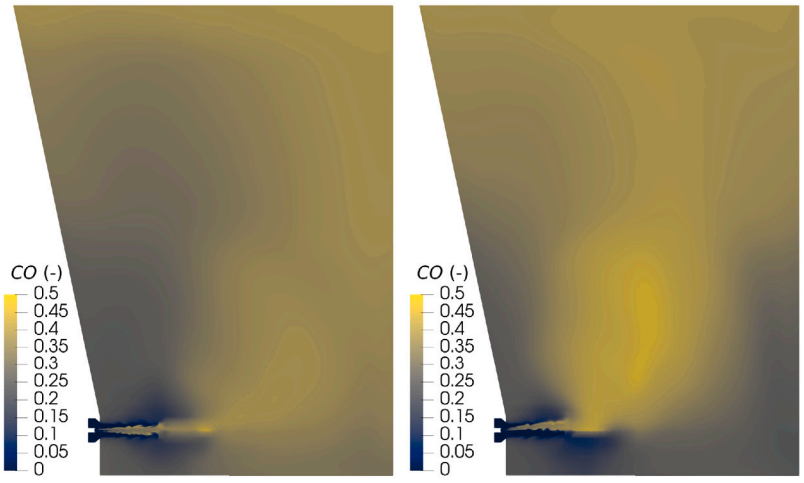

(c) CO 0° lance configuration. (d) CO +13° lance configuration.

Fig. 13. Cross-sectional snapshots of O_2 and CO mass fraction at pseudo steady state.

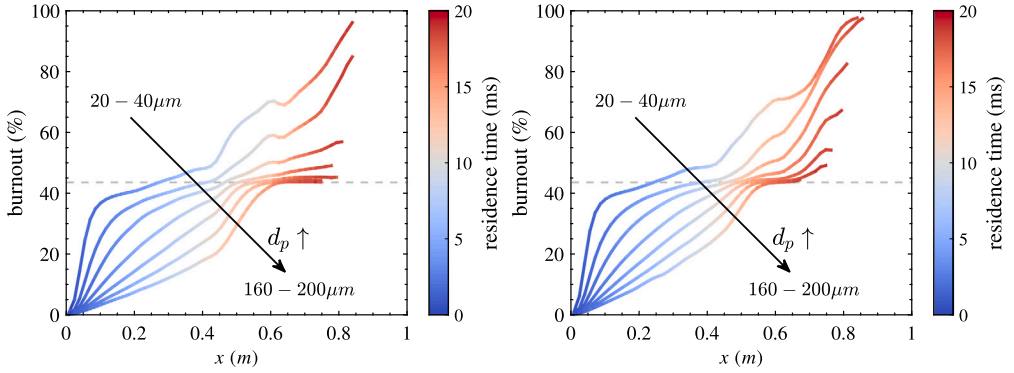

(a) 0° lance configuration. (b) +13° lance configuration.

Fig. 14. Burnout in different particle size groups, from 20-40 µm, 40-60 µm, 60-80 µm, 80-100 µm, 100-120 µm, 120-160 µm, and 160-200 µm. Each line displays information averaged within the corresponding particle size group. The gray dashed line indicates burnout contribution from the devolatilization. (a) 0° lance configuration. (b) +13° lance configuration.

the physical raceway, resulting in stagnation due to the resistance of the coke bed. The location of these unburned PC particles closely corresponds to the bird's nest region commonly observed in industrial blast furnaces. This finding highlights the necessity for considering both coke and PC as colliding entities in order to capture this accumulation of PC or char/ash within the coke channels. However, long-term simulations would be required for understanding the effects of the char/PC accumulation on the char paths through the BF and thereby on the conversion, and vice versa the effect of bird's nest on raceway formation.

By varying the pulverized coal injection (PCI) rate, from zero to 0.6 kg/s, the shape and size of the physical raceway within a short timescale are found to be primarily determined by the thrust of the blast air.

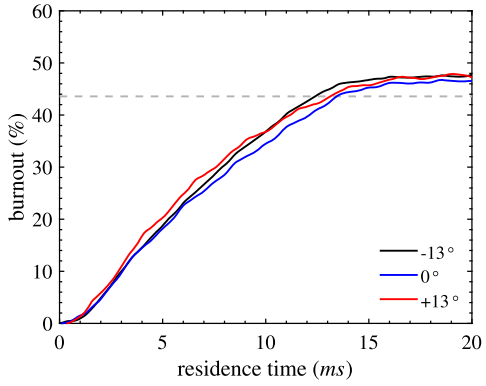

Fig. 15. Time-averaged overall PC burnout from three lance configurations. The gray dashed line indicates burnout contribution from the devolatilization. The calculation of the overall burnout is the same as that in Fig. 11 except that residence times other than 20 ms are also considered.

The contribution of gas expansion from the PC combustion is negligible to the physical raceway dimension in the simulations with current geometrical setup. The chemical raceway shrinks little with an increasing PCI rate (0.2 kg/s to 0.6 kg/s) because the mixing of PC with O_2 does not improve with increasing PCI rate. From the simulations, the overall burnout of PC is found to be irrelevant to the varying PCI lance angle, although the chemical raceway shape and size differ. When the lance angle is +13°, the CO distribution is more homogeneous in the upper part of the domain.

The simulations have revealed several aspects associated with the raceway formation within an injection zone of a blast furnace, including the formation of the physical and chemical raceway, the utilization and trajectory of PC, the effect of PCI rate, and the impact of lance configuration. To improve PC utilization, it is essential to enhance PC-blast mixing which however cannot be simply achieved by modifying the lance angle nor increasing the PCI rate. These findings offer new insights into the optimization of the blast furnace operations and establish the basis for future research.

CRediT authorship contribution statement

Chih-Chia Huang: Conceptualization, Investigation, Methodology, Writing – original draft. **Stefan Born:** Resources, Supervision, Writing – review & editing. **Margot Klaassen:** Investigation, Supervision. **Jeroen A. van Oijen:** Investigation, Methodology, Supervision, Writing – review & editing. **Niels G. Deen:** Conceptualization, Investigation, Methodology, Project administration, Supervision, Writing – review & editing. **Yali Tang:** Conceptualization, Funding acquisition, Investigation, Methodology, Supervision, Writing – review & editing.

Declaration of competing interest

The authors declare the following financial interests/personal relationships which may be considered as potential competing interests:

Yali Tang reports financial support was provided by M2i Materials Innovation Institute. If there are other authors, they declare that they have no known competing financial interests or personal relationships that could have appeared to influence the work reported in this paper.

Data availability

Data will be made available on request.

Acknowledgements

This work was carried out on the Dutch national e-infrastructure with the support of SURF Cooperative and under project number T18021 in the framework of the Research Program of the Materials innovation institute (M2i) (www.m2i.nl) supported by the Dutch government. Financial support by Tata Steel Nederland is gratefully acknowledged.

References

IEA, 2022. Iron and steel. https://www.iea.org/reports/iron-and-steel.
Geerdes, M., Chaigneau, R., Lingiardi, O., 2020. Modern Blast Furnace Ironmaking: An Introduction (2020). Ios Press.
IEA, 2020. Iron and Steel Technology Roadmap. Iron and Steel Technology Roadmap.
UNFCCC, 2021. COP 26 Glasgow climate pact advance unedited version decision. In: Cop26, pp. 1–8.
Umekage, T., Yuu, S., Kadowaki, M., 2006. Numerical simulation of blast furnace raceway depth and height, and effect of wall cohesive matter on gas and coke particle flows. ISIJ Int. 45, 1416–1425.
Wright, B., Zulli, P., Zhou, Z.Y., Yu, A.B., 2011. Gas-solid flow in an ironmaking blast furnace - I: physical modelling. Powder Technol. 208, 86–97.
Hilton, J.E., Cleary, P.W., 2012. Raceway formation in laterally gas-driven particle beds. Chem. Eng. Sci. 80, 306–316.
Rangarajan, D., Shiozawa, T., Shen, Y., Curtis, J.S., Yu, A., 2014. Influence of operating parameters on raceway properties in a model blast furnace using a two-fluid model. Ind. Eng. Chem. Res. 53, 4983–4990.
Hou, Q., E, D., Yu, A., 2016. Discrete particle modeling of lateral jets into a packed bed and micromechanical analysis of the stability of raceways. AIChE J. 62, 4240–4250.
Miao, Z., Zhou, Z., Yu, A.B., Shen, Y., 2017. CFD-DEM simulation of raceway formation in an ironmaking blast furnace. Powder Technol. 314, 542–549.
Rabadan Santana, E., Pozzetti, G., Peters, B., 2019. Application of a dual-grid multiscale CFD-DEM coupling method to model the raceway dynamics in packed bed reactors. Chem. Eng. Sci. 205, 46–57.
Shen, Y.S., Guo, B.Y., Yu, A.B., Austin, P.R., Zulli, P., 2011. Three-dimensional modelling of in-furnace coal/coke combustion in a blast furnace. Fuel 90, 728–738.
Shen, Y.S., Yu, A.B., Austin, P.R., Zulli, P., 2012. CFD study of in-furnace phenomena of pulverised coal injection in blast furnace: effects of operating conditions. Powder Technol. 223, 27–38.
Shen, Y., Shiozawa, T., Austin, P., Yu, A., 2014. Model study of the effect of bird's nest on transport phenomena in the raceway of an ironmaking blast furnace. Miner. Eng. 63, 91–99.
Shen, Y., Yu, A., 2015. Characterization of coal burnout in the raceway of an ironmaking blast furnace. Steel Res. Int. 86, 604–611.
Zhuo, Y., Shen, Y., 2020. Three-dimensional transient modelling of coal and coke co-combustion in the dynamic raceway of ironmaking blast furnaces. Appl. Energy 261, 114456.
Cui, J., Hou, Q., Shen, Y., 2020. CFD-DEM study of coke combustion in the raceway cavity of an ironmaking blast furnace. Powder Technol. 362, 539–549.
Xu, D., Wang, S., Shen, Y., 2022. An improved CFD-DEM modelling of raceway dynamics and coke combustion in an industrial-scale blast furnace. Chem. Eng. J., 140677.
Van Oijen, J.A., Lammers, F.A., De Goey, L.P., 2001. Modeling of complex premixed burner systems by using flamelet-generated manifolds. Combust. Flame 127, 2124–2134.
Benyahia, S., Janine, G., 2010. Estimation of numerical errors related to some basic assumptions in discrete particle methods. Int. J. Numer. Methods Fluids 49, 10588–10605.
Radl, S., Radeke, C., Khinast, J.G., Sundaresan, S., 2011. Particle-based approach for the simulation of gas-particle flows, 1–10.
Weller, H.G., Tabor, G., Jasak, H., Fureby, C., 1998. A tensorial approach to computational continuum mechanics using object-oriented techniques. Comput. Phys. 12, 620.
Kloss, C., Goniva, C., Hager, A., Amberger, S., Pirker, S., 2012. Models, algorithms and validation for opensource DEM and CFD-DEM. Prog. Comput. Fluid Dyn. 12, 140.
Huang, C.-C., van Oijen, J.A., Deen, N.G., Tang, Y., 2022. Incorporation of flamelets generated manifold method in coarse-grained Euler-Lagrange simulations of pulverized coal combustion. Chem. Eng. Sci., 117838.
Beetstra, R., van der Hoef, M.A., Kuipers, J.A.M., 2007. Drag force of intermediate Reynolds number flow past mono- and bidisperse arrays of spheres. AIChE J. 53, 489–501.
Ishii, K., 2000. Advanced Pulverized Coal Injection Technology and Blast Furnace Operation. Elsevier.
Badzioch, S., Hawksley, P.G., 1970. Kinetics of thermal decomposition of pulverized coal particles. Ind. Eng. Chem. Process Des. Dev. 9, 521–530.
Baum, M.M., Street, P.J., 1971. Predicting the combustion behaviour of coal particles. Combust. Sci. Technol. 3, 231–243.
Kashiwaya, Y., Ishii, K., 1991. Kinetic analysis of coke gasification based on non-crystal/crystal ratio of carbon. ISIJ Int. 31, 440–448.
Merrick, D., 1983. Mathematical models of the thermal decomposition of coal. 2. Specific heats and heats of reaction. Fuel 62, 540–546.
Tomeczek, J., Palugniok, H., 1996. Specific heat capacity and enthalpy of coal pyrolysis at elevated temperatures. Fuel 75, 1089–1093.
Somers, B., 1994. The simulation of flat flames with detailed and reduced chemical models. Ph. D. Dissertation. 195.

Smith, G.P., Golden, D.M., Frenklach, M., Moriarty, N.W., Eiteneer, B., Goldenberg, M., Bowman, C.T., Hanson, R.K., Song, S., Gardiner, W.C., Jr., V.V.L., Qin, Z., 1999. GRI-Mech 3.0. http://combustion.berkeley.edu/gri-mech/version30/text30.html.

Poletto, R., Craft, T., Revell, A., 2013. A new divergence free synthetic eddy method for the reproduction of inlet flow conditions for les. Flow Turbul. Combust. 91, 519–539.

Deb, S., Tafti, D.K., 2013. A novel two-grid formulation for fluid-particle systems using the discrete element method. Powder Technol. 246, 601–616.

Farzaneh, M., Sasic, S., Almstedt, A.E., Johnsson, F., Pallarès, D., 2011. A novel multi-grid technique for Lagrangian modeling of fuel mixing in fluidized beds. Chem. Eng. Sci. 66, 5628–5637.

Pozzetti, G., Besseron, X., Rousset, A., Peters, B., 2018. A co-located partitions strategy for parallel CFD–DEM couplings. Adv. Powder Technol. 29, 3220–3232.

Gupta, G.S., Rajneesh, S., Rudolph, V., Singh, V., Sarkar, S., Litster, J.D., 2005. Mechanics of raceway hysteresis in a packed bed. Metall. Mater. Trans., B Process Metall. Mater. Proc. Sci. 36, 755–764.

Nishi, T., Haraguchi, H., Miura, Y., Sakurai, S., Ono, K., Kanoshima, H., 1982. Relationship between shape of raceway and productivity of blast furnace taking account of properties of coke sampled at tuyere level. Trans. Iron Steel Inst. Jpn. 22, 287–296.

Atkinson, C.J., Willmers, R.R., 1990. Blast furnace coal injection studies using a single tuyere raceway investigation rig. Fuel Process. Technol. 24, 107–115.

Jamaluddin, A.S., 1985. Combustion of Pulverised Coal as a Tuyere-Injectant to Blast Furnace. University of Newcastle, Newcastle.

Majeski, A., Runstedtler, A., D'Alessio, J., Macfadyen, N., 2015. Injection of pulverized coal and natural gas into blast furnaces for iron-making: Lance positioning and design. ISIJ Int. 55, 1377–1383.

Wu, D., Shi, P., Zhou, P., Zhou, C.Q., Yan, H., 2018. Numerical investigation of the effects of size segregation on pulverized coal combustion in a blast furnace. Powder Technol. 342, 41–53.

Ariyama, T., Sato, M., Yamakawa, Y.i., Yamada, Y., Suzuki, M., 1994. Combustion behavior of pulverized coal in tuyere zone of blast furnace and influence of injection lance arrangement on combustibility. Tetsu-To-Hagane/J. Iron Steel Inst. Jpn. 80, 34–39.